Ultrasonics Sonochemistry 83 (2022) 105939

Contents lists available at ScienceDirect

Ultrasonics Sonochemistry

journal homepage: www.elsevier.com/locate/ultson

Sonoluminescence emission spectra of a 3.6 MHz HIFU in sweeping mode

Noura Sleiman [a,b,c], Loïc Hallez [a], Rachel Pflieger [b], Sergey I. Nikitenko [b], Jean-Yves Hihn [a,c,*]

[a] UTINAM UMR 6213, Univ Bourgogne-Franche-Comté/CNRS, Besançon, France
[b] ICSM UMR 5257 – CEA, Univ Montpellier, CNRS, ENSCM, Bagnols-sur-Cèze, France
[c] IRT M2P, Metz, France

ARTICLE INFO

Keywords:
HIFU
Frequency sweep
Cavitation
Sonoluminescence
Emission spectra

ABSTRACT

Use of sweeping mode with a 3.6 MHz High Intensity Focused Ultrasound (HIFU) allows cavitation activity to be controlled. This is especially true in the pre-focal zone where the high concentration of bubbles acts as an acoustic reflector and quenches cavitation above this area. Previous studies attributed the enhancement of cavitation activity under negative sweep to the activation of more bubble nuclei, requiring deeper investigations. After mapping this activity with SCL measurements, cavitation noise spectra were recorded. The behavior of the acoustic broadband noise follows the sonochemical one i.e., showing the same attenuation (positive scan) or intensification (negative scan) of cavitational activity. In 1 M NaCl 3.7 mM 2-propanol solution saturated by a mixture of Ar-15.5%O_2-2.2%N_2, intensities of SL spectra are high enough to allow detection of several molecular emissions (OH, NH, C_2, Na) under negative frequency sweeps. This is the first report of molecular emissions at such high frequency. Their intensities are low, and they are very broad, following the trend obtained at fixed frequency up to 1 MHz. Under optimized conditions, CN emission chosen as a spectroscopic probe is strong enough to be simulated, which is reported for the first time at such high frequency. The resulting characteristics of the plasma do not show any spectral difference, so bubble nature is the same in the pre-and post-focal zone under different sweeping parameters. Consequently, SL and SCL intensification was not related to a change in plasma nature inside the bubbles but to the number of cavitation bubbles.

1. Introduction

Acoustic cavitation – formation, growth, and implosive collapse of bubbles in liquids irradiated with high intensity ultrasound – is the source of various mechanical and chemical phenomena [1]. In particular, the violent collapse of bubbles generates high temperatures and pressures (up to thousands of Kelvins and hundreds of bars) inside the bubbles, and these 'hot spots' form the position of the so-called sonochemistry [2–4]. Studying sonoluminescence emission spectra is a powerful assay tool for bubble temperature determination during cavitation [5]. Flint and Suslick estimated a 'cavitation temperature of about 5000 K [2], while vibrational temperatures T_v of OH excited species were reported to be about 10,000 K in argon-saturated water [6].

Sonoluminescence of aqueous and non-aqueous solutions has been widely investigated in recent decades [2,3,7,8]. It has been shown that several experimental conditions, such as ultrasonic frequency, nature of solvent and of dissolved gas, affect the number of sonoluminescent bubbles and plasma conditions, as well as sonochemical efficiency [9–11]. Concerning the effect of salt, Lepoint-Mullie et al. demonstrated that it can enter the bubbles by droplet injection (which results in the emission of alkali-metal species in the SL of aqueous solutions of salts) [7]. This impact of salt on sonochemical and sonoluminescence yields was also highlighted by more recent studies [12]. Other solutes are reported to modify the SL spectrum and intensity, such as alcohols (e.g. *tert*-butyl alcohol), degradation of which leads to the emission of C_2 Swan bands, a well-known spectroscopic probe [13,14].

However, among these the role of the dissolved gas is of particular interest. Considering pure gases, the highest SL intensity is attained under noble gases due, in particular, to their high adiabatic ratio [15], to their low ionization potential [16] and to the fact that their reactions in the bubbles are limited. SL intensity increases with the atomic weight of the noble gas, due to decreasing thermal conductivity and increasing solubility [17,18]. Besides, the addition of 20–30% O_2 in Ar can increase production of OH radicals and SL intensity [9,10].

The plasma generated during sonication can be characterized by the fitting of molecular emissions, the shape of which is a fingerprint of both the plasma characteristics and the chemical reactions leading to the formation of the excited species [19]. Already in pure water, several

* Corresponding author.
E-mail address: jean-yves.hihn@univ-fcomte.fr (J.-Y. Hihn).

https://doi.org/10.1016/j.ultsonch.2022.105939
Received 20 December 2021; Received in revised form 26 January 2022; Accepted 28 January 2022
Available online 1 February 2022

molecular bands can be observed. For example, sonolysis of water under argon gas leads to the observation of OH (A-X) around 310 nm [7]. The latter emission also appears under Ar-5%N_2, Ar-0.5%CO_2 and Ar-0.5% CO_2-5%N_2, while NH (A-X) emission at 337 nm is present under Ar-5% N_2 mixture [19]. In the presence of Ar-0.5% CO_2-5%N_2 CN bands are clearly visible around 386 nm. Use of this gas mixture also leads to emission of C_2 Swan bands.

Ultrasonic frequency impacts sonoluminescence and plasma conditions in a number of ways [20]. At low frequencies, bubbles will be larger and will more readily demonstrate surface instability. Yasui [21] reported that the ambient bubble radius at 20 kHz calculated in Ar saturated water is 0.1–100 μm, while at a higher frequency of 1 MHz it is 0.1–3 μm. It was also reported that OH rovibronic temperatures increase with US frequency [10]. Thus, varying sonication frequency appears to be a real issue. The number of cavitation bubbles increases at higher frequencies although higher powers are needed to produce active bubbles, mainly because at high frequencies bubbles have less time to grow and to collapse [22]. A recent study demonstrated that sonoluminescence spectral shape of 100 kHz is similar to that at 20 kHz with a very intense, well defined OH ($A^2\Sigma^+ - X^2\Pi$) emission and a relatively low continuum, contrary to high frequency SL spectra where the continuum is intense and molecular emissions broad [6]. Nevertheless, spectroscopic studies have never been investigated beyond 1 MHz, so there is no data on the temperature reached inside the bubbles during cavitation at ultrasonic frequency above 1 MHz. The reason is the limitation of the available energy that can be used for transducer excitation in these conditions, where transducer thickness drastically decreases, thereby causing thermal issues and difficulties in cavitation ignition.

A solution resides in acoustic energy concentration by using high-intensity focused ultrasound (HIFU) which allows acoustic energy to be focused up to cavitation threshold at a focal point for a wide range of high frequencies (1 MHz to 4 MHz). Even when cavitation is not reached, absorption of the acoustic energy generates remarkable heating at the focal point, finding therapeutic applications [23,24] or applications in surface treatment [25]. Hallez et al. extensively described distribution of acoustic energy and cavitational activity [26], as well as hydrodynamic behavior in the HIFU sonoreactors [27]. They determined acoustic field distribution and localized the areas of interest by comparing complementary technics such as modeling, hydrophone measurements, laser tomography, and SCL measurements. Contrary to expectations, the main activity was not detected at the acoustic focal point but in the pre-focal zone (between the HIFU and the focal zone). Nevertheless, an activity could be detected in the post-focal zone on the outer layer of the propagation cone for very high powers [26]. This was confirmed by velocity vector fields highlighted by Particle Image Velocimetry (PIV), as well as by electrochemical measurements. The latter quoted in equivalent velocities quantified the deviation from the theoretical values deduced from Eckart's equation, and explain the behavior in the zone just before the geometrical focal [27]. Chen et al. showed with high speed camera records that the bubbles present in the focal zone act as a reflector for acoustic wave propagation, shifting the activity towards the transducer [28]. Bubble size distribution was measured at fixed frequencies by pulsed experiments [29], and radii obtained for 3.6 MHz in air saturated water were about 0.76 to 1.03 μm [30].

However, the most recent discovery concerned control of the HIFU excitation signal. The UTINAM institute has developed a technique able to either strongly enhance or quench the cavitation activity of the HIFU by sweeping frequency (wobbling) [27]. It was shown that, irrespectively of the frequency gap, it is the direction and, to a lesser extent, the frequency sweep rate which govern light production by both sonoluminescence and sonochemiluminescence. Indeed, an unprecedented enhancement is observed when frequency is swept in reverse (negative sweep), while a positive sweep results in a quenching of both SL and SCL [27,30]. Finally, this technique applied to HIFU allows interesting control of cavitation activity in the sonoreactor, thus significantly widening the perspective of ultrasound use at very high frequencies.

The present work intends to conduct a spectroscopic study at an unexplored frequency range (3.6 MHz) thanks to the use of frequency sweep and HIFU transducer shape. An important issue resides in the plasma characteristics (illustrated in molecular emissions in sonoluminescence) in a range of frequencies never studied and in the particular effect of frequency sweep. To this end, a specific sonoreactor adapted to spectroscopy measurements and allowing gas control was built and characterized with sonochemiluminescence to identify the most active zone. Then, several experimental parameters (nature of gases and chemical additives, frequency sweep parameters) were varied to perform SL measurements, determine luminescence activity, and give some insight into the conditions attained.

2. Experimental details

2.1. Materials

All aqueous solutions were prepared with deionized water (Milli-Q 18.2 MΩ cm) at ambient temperature and a volume of 300 mL. Reagents and chemicals used in the various procedures were all of analytical grade and were purchased from Sigma Aldrich, except for sodium chloride salts purchased from VWR Chemicals BDH. Argon at 99.999% purity, Ar-20% O_2, Ar-10%N_2 and Ar-1%CO_2 were provided by Air Liquide. The pH of luminol solutions was adjusted to 10.8 by adding Na_2CO_3.

2.2. Experimental procedures

The set-up consists of a thermostated glass-made batch reactor installed on top of a High-Intensity-Focused-Ultrasound (HIFU) designed by IMASONIC (Besançon, France) placed in a black box Fig. 1 [31]. The bandwidth of the HIFU used is between 2 and 5 MHz where maximum performance is achieved at a frequency of 4.0 ± 0.4 MHz (Fig. 1SI in Supporting information). A multifrequency generator controlled the HIFU, in which the signal was first amplified before reaching the transducer. Temperature in the reactor during irradiation was adjusted to 10 °C using a Huber Unistat Tango thermo-cryostat [10]. For all experiments, the solutions were injected with gas (Ar; Ar-20%O_2; Ar-0.5%CO_2-5%N_2 or Ar-15.5%O_2-2.2%N_2) about 30 min before ultrasonic sonication (with the gas inlet tube placed in the center of the sonoreactor) and during the ultrasonic treatment (after moving the inlet tube to the reactor's side), at a steady flow rate of 60 mL min-1. The gas flow rates were monitored using a double-entry volumetric flow meter with stainless-steel float (Aalborg) [11] that also allowed in-situ preparation of gas mixtures. Electrical power was 33 W corresponding to an absorbed acoustic power of 7 ± 1 W, measured by calorimetric method, while the position of the thermocouple was chosen to avoid it being directly heated by absorption of ultrasound [32]. This power was kept constant for all sweeping conditions except in the measurement of acoustic spectra. Light emission spectra of sonoluminescence (SL) were collected through a flat quartz window using Al coated parabolic mirrors and recorded using a Roper Scientific SP 2356i spectrometer (gratings 150blz500 and 600blz300, slit width 0.1 mm) coupled to a UV-coated CCD camera (SPEC10-100BR Roper Scientific) cooled by liquid nitrogen. For each SL experiment, at least three 900-s spectra were averaged and corrected for background noise and the quantum efficiencies of grating and CCD [19]. When needed, a high-pass filter cutting at 320 nm was used to avoid second order emissions. Specair software was used to fit the molecular emissions, the process parameters were the vibrational and rotational temperatures (T_v and T_r) of the relevant species, gas temperature was taken equal to T_r, and effective pressure was P.

Sonochemiluminescence (SCL) images were taken through the flat quartz window with a Canon EOS 100D digital camera (diaphragm aperture F5.6, sensitivity ISO 3200, exposure time 1 min). Acquisition was performed with Digital Photo Professional software. The luminol

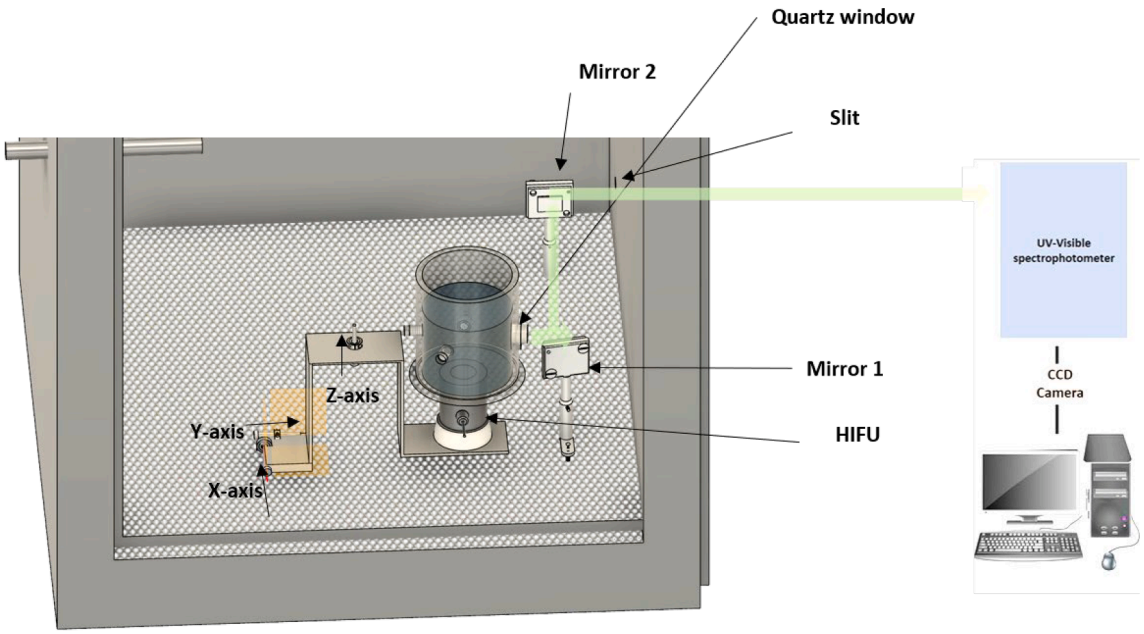

Fig. 1. Drawing of the set-up of SL experiments.

solution was saturated under a continuous Ar-20 %O_2 flow for 30 min before starting sonication. Photos were captured after a few minutes of sonication. The images were processed with Matlab® to sum the intensities of the 3 colors (RGB) for each line of the picture [26]. A luminosity curve along the acoustic axis was obtained. Lastly, a smoothing step and background noise subtraction were performed.

The acoustic spectra of the cavitational fields were recorded for different wobbling parameters with a hydrophone (ICA 3 MHz from the University of Minsk) coupled to an oscilloscope (Lecroy WaveSurfer 44Xs, 400 MHz, 2.5 GS/s). Measurement consisted in recording the noise generated by cavitation by placing a hydrophone at the peripheral edge of the acoustic field in the sonoreactor filled with air-saturated demineralized water. After averaging 1000 sweeps, the Fast Fourier Transform of the signals was used to establish the acoustic spectra. Collected data were processed by Matlab® following different treatment steps: subtraction of background noise (using a spectrum without US). The area under the curve of the acoustic spectrum was also calculated by removing the harmonics and the fundamental frequency and then integrating the curve to finally obtain the broadband noise.

In the present work, different sweep parameters were used: frequency sweep range Δ F (Eq. (2)) that can be negative ($F_{stop} > F_{start}$) or positive ($F_{stop} < F_{start}$), sweep period T_{sweep} and sweep rate r_{sweep} (Eq. (3)).

$$\Delta F = F_{stop} - F_{start}\ (\mathrm{MHz}) \tag{2}$$

$$r_{sweep} = \frac{\Delta F}{T_{sweep}}\ (\mathrm{MHz/s}) \tag{3}$$

3. Results and discussion

3.1. Localization and quantification of cavitation activity

Sonochemiluminescence of luminol has been used in the past for identification of sonochemically active areas due to the reaction of free radicals, resulting from the implosion of bubbles, in presence of luminol. This technique has been successfully used to characterize the cavitation field in HIFU sonoreactors but only at fixed frequency [26]. In this paper, it is further used for sweep conditions, where several parameters can be controlled: start and stop frequencies and sweep period which determine sweep direction and rates. These parameters influence the evolution and distribution of global intensity but may also act in SCL distribution on both sides of the focal zone [30].

Fig. 2a presents the SCL emission of luminol in a representative case of wobbling for a 0.01 M luminol solution (pH = 10.8, Na_2CO_3), under bubbling of Ar-20%O_2. It allowed us to clearly identify two chemically active zones (blue zones) along the z-axis (Fig. 1 and 2a): the zone above the focal or post-focal and the zone below the focal or pre-focal zone separated by the acoustic focal situated in the black zone (H = 0 mm). This corresponds to previous observations with HIFU which revealed the same conical SCL shape [25], bubble behavior [26], and the dynamics of cavitation bubble clouds [28,33,34]. Fig. 2b represents brightness curves for SCL images taken under a fixed F_{start} at 3.6 MHz and a sweep time from 1 ms to 5 ms with a rate of −80 MHz/s and +80 MHz/s for 5 ms. The first peak (small) corresponds to the post-focal zone, while the highest peak (second peak) corresponds to the pre-focal zone. We noticed that the highest peak is obtained at 1 ms for both the post-focal zone and the pre-focal zone. It is important to notice that SCL intensity, at the same power but at fixed frequency (resonance frequency) is near zero, thus confirming wobbling efficiency in triggering cavitation, particularly for the post-focal zone where short periods are required for SCL ignition.

Previous works at fixed frequency have shown that at low powers, cavitational activity is concentrated in the pre-focal zone. Increasing the power triggers the appearance of another luminescent cloud in the post-focal zone [34]. The appearance of SCL under the focal zone was explained by the dynamics of the bubble cloud during the first instants by images captured at high-speed [34], while the absence of SCL in the post-focal zone at lower powers is due to the focal zone acting as a propagation barrier in the first milliseconds, reflecting the acoustic wave back to the transducer. The superposition of reflected and incident waves tends to shift the bubble cloud towards the pre-focal zone.

The impact of sweep period is shown in Fig. 3 under a fixed F_{start} at 3.6 MHz and a constant rate at −80 MHz/s: increasing the period of wobbling from 1 ms to 5 ms leads to a decrease in activity and to changes in SCL light distribution. In particular, the post-focal zone shows SCL for some periods, while it is dark for some others. In accordance with Fig. 2b, photon emission is low on the acoustic axis in the post-focal region. The traces of SCL in this area are due to the combined action of Bjerknes forces, acoustic currents, and the radiation force acting on the initial bubble cloud. Bubbles created in the focal zone are driven in

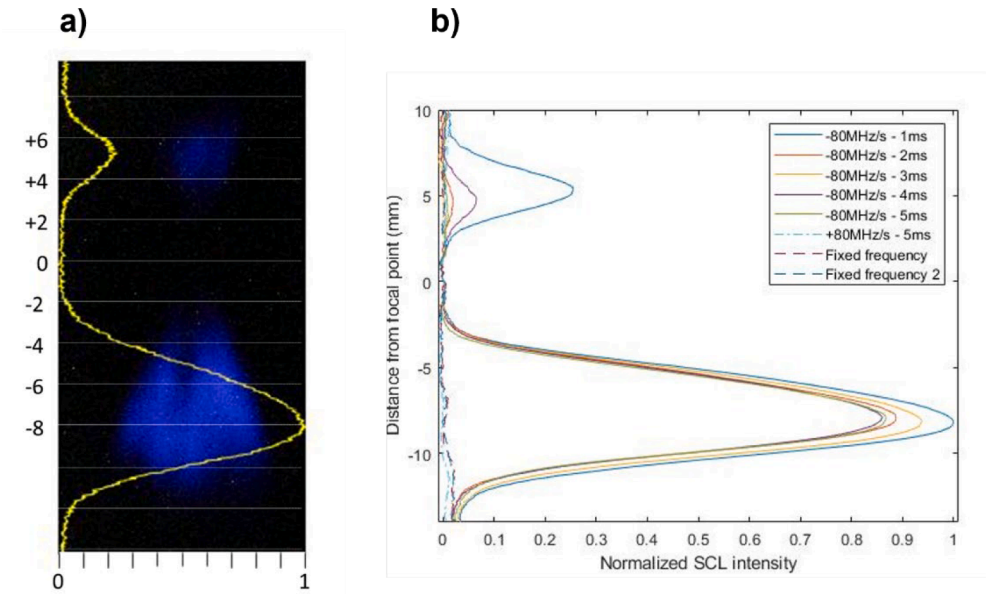

Fig. 2. (a) Normalized brightness for a photography of the SCL of 300 mL of 0.01 M luminol solution (pH = 10.8, Na_2CO_3), Ar-20%O_2, exposure time 1 min at 3600 kHz −80 MHz/s (1 ms) in accordance with the height H (vertical axis) considering 0 as the focal point. (b) Brightness curves for SCL images taken under different wobbling periods and rates.

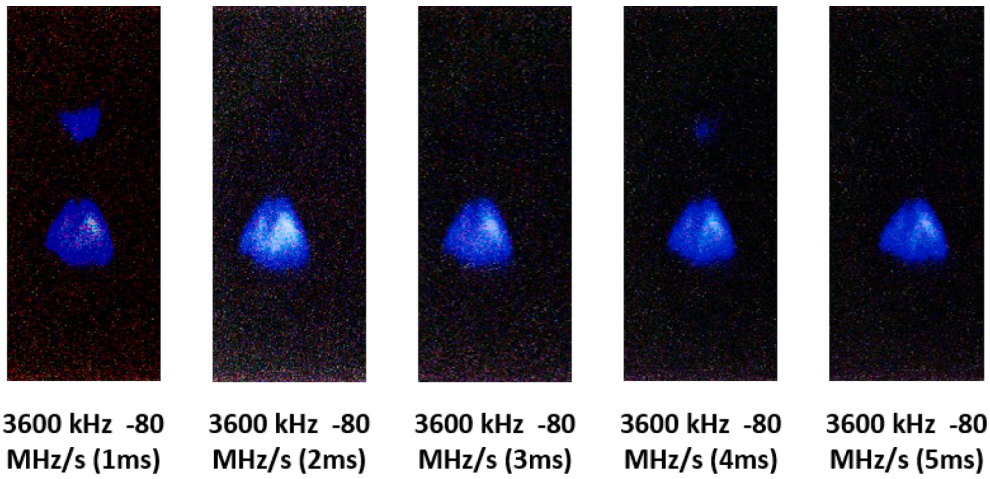

Fig. 3. SCL imagery with luminol (0.01 M, pH = 10.8, Na_2CO_3), Ar-20%O_2, iso 3200, 1-minute duration, using a Canon EOS 100 D camera.

the direction of wave propagation by these forces, and luminescence occurs in the post-focal zone. Yet, an absence of SCL can be noted in the focal region due to the energy losses induced by bubble density at the focal point, known as oversaturation phenomena [32].

Besides, the numbers of active bubbles in the two zones appear not to be correlated. There is no SCL activity detected under positive scan (Fig. 2 and Fig. 2SI in Supporting information). Starting frequency does not affect distribution of the sonochemical activity. Results confirm that the pre-focal zone is brighter than the post-focal zone and thus more active. Therefore, quantification is required, and SCL images under different conditions (sweep time and direction of the scan) were treated by MATLAB to integrate the area under luminescent distribution curves.

Integrated luminosity was normalized at 1 for a fixed frequency of 3.6 MHz (Fig. 4) for different F_{stop} between 3.2 and 4 MHz under 3.6 MHz as F_{start}. The gray dots representing negative wobbling ($\Delta F < 0$) showed a 10 times higher integrated luminosity than at fixed frequency $\Delta F = 0$ and positive wobbling ($\Delta F > 0$, white dots). These measurements illustrated that sonochemical activity was markedly improved for negative wobbling rates, especially for short sweeping periods (1 ms).

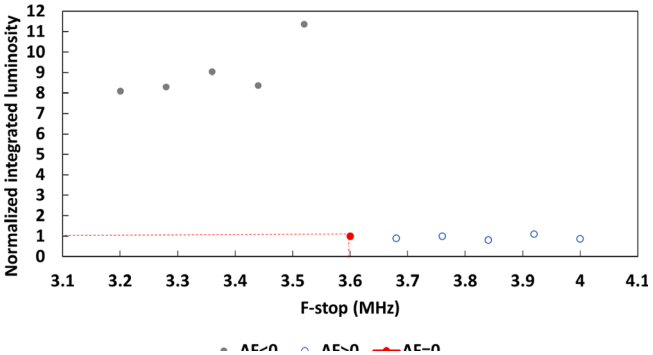

Fig. 4. Integrated luminosity normalized at 1 for fixed frequency 3.6 MHz for different F_{stop} with F_{start} = 3.6 MHz and rate of ±80 MHz/s at 200 mV: $\Delta F > 0$ for positive sweeps, $\Delta F < 0$ for negative sweep.

As a complement, acoustic spectra of the cavitational fields were recorded as illustrated in Fig. 5 at a fixed frequency of 3.6 MHz. When input power increased from 100 mV (Fig. 5a) to 200 mV (Fig. 5b), with corresponding electrical effective powers of 8 W and 28 W respectively, harmonics ($2f_0$, $3f_0$ …), subharmonics ($f_0/2$, $f_0/3$ …), and ultra-harmonics ($3f_0/2$ …) were more clearly visible in the spectrum, indicating the presence of cavitation bubbles [35–37]. Broadband noise was defined by integration of the area under the acoustic spectra curves, and is presented in Fig. 6 for different F_{stop} between 3 and 4 MHz with a F_{start} of 3.6 MHz and a scan rate of ±80 MHz/s. It is interesting to note that they behave in the same manner as SCL (Fig. 4): quenched by the positive frequency sweep and enhanced for the negative frequency sweeps, especially for large gaps. This highlights the contribution of inertial cavitation, including stable oscillation and most bubble collapses. Moreover, a decrease in intensification for longer wobbling times is seen, which confirms results obtained in previous studies [30]. In addition, oscillation regimes can be characterized by subharmonics and ultraharmonics frequency analysis. This includes $3f_0/2$, the non-linear signatures of stable cavitation bubble oscillations, which is plotted in Fig. 7 and presents the same behavior [38,39]. The different behaviors observed for the pre- and post-focal zones, their different SCL intensities and sensitivities to wobbling parameters question the nature of the bubbles formed in both zones. Indeed, changes in SCL intensity may be due either to changes in the active bubble number or to changes in the nature of bubbles, in the conditions reached in their core at collapse. To probe the latter, SL emission spectra were measured for different wobbling conditions.

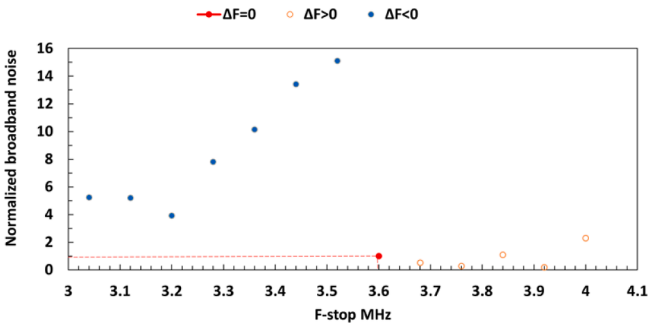

Fig. 6. Intensity of the broadband noise of acoustic spectra. Results are normalized at 1 for fixed frequency 3.6 MHz for different F_{stop} with F_{start} = 3.6 MHz and rate of ±80 MHz/s at 200 mV: ΔF > 0 for positive sweeps, ΔF < 0 for negative sweep.

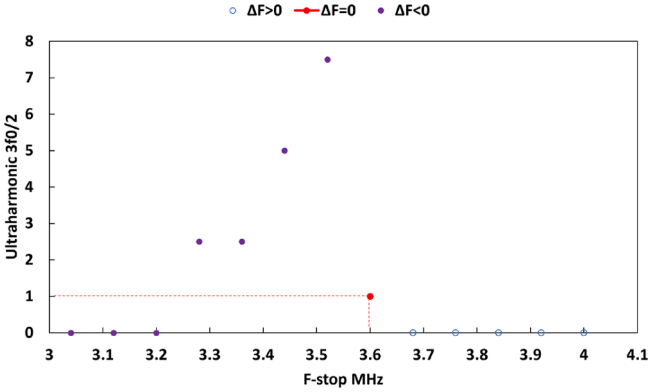

Fig. 7. Intensity of the Ultraharmonic $3f_0/2$ for different acoustic spectra corresponding to different F_{stop} with F_{start} = 3.6 MHz and rate of ±80 MHz/s. Results are normalized at 1 for fixed frequency 3.6 MHz at 200 mV: ΔF > 0 for positive sweeps, ΔF < 0 for negative sweep.

3.2. Finding a spectroscopic probe

Measurement of SL spectra at very high frequency, even with focused US, is a challenging task due to the very dim emission. Indeed, SL intensity markedly decreases when US frequency is above approx. 400 kHz [40]. For this reason, the measured system must be chosen so as to increase SL intensity as much as possible. Only aqueous solutions were considered to allow comparison with the luminol SCL study and because they are the most relevant for HIFU applications. Presence of 1 M NaCl salt in aqueous solutions is known to increase the intensity of sonoluminescence [12,41], in particular by decreasing dissolved gas concentration and consequently bubble coalescence and formation of big degassing bubbles [12]. The latter property of salt also ensures reproducibility of the measurement by avoiding formation of big bubbles on the HIFU membrane. Second, the measured system should be chosen to allow observation of molecular emissions with the aim of fitting them with spectroscopy software to get rovibronic temperatures of the excited species, or in other words some information on the formed plasma. In a previous study, we showed that the 362 kHz SL spectra of water saturated with Ar-5%N_2-0.5%CO_2 gas mixture [19] bore clear molecular emissions of OH, C_2 and CN. Unfortunately, SL spectra of water saturated with this gas mixture were extremely dim at 4 MHz (Fig. 3SI A in Supporting Information), whichever wobbling conditions were tested. This very low intensity was traced back to quenching of SL by CO_2 molecules (as was previously observed [42]), even at this low concentration. Thus, another approach had to be adopted to measure some molecular emissions, aiming at the already reported emissions of OH, NH, C_2 and CN. First, gas nature was modified to Ar-15.5%O_2-2.2%N_2. Indeed, an O_2 content in Ar around 20% was previously shown to yield a maximum in SL intensity, in a large range of frequencies [10,43,44]. This effect was also observed in the present conditions (Fig. 3SI C in Supporting Information). N_2 was added as a source of N atoms, necessary to form NH and CN species. Finally, to avoid CO_2, an alternative source of carbon was added to the solution, namely 2-propanol. Its concentration (3.7 mM) was chosen according to previous studies [14,19], high enough to allow formation and emission of CN (and a priori C_2) but low enough to limit SL quenching. The resulting SL spectra (Fig. 8a and b) indeed presented several emissions (OH, CN, C_2, Na), though not very intense and very broad. The very low intensity of Na

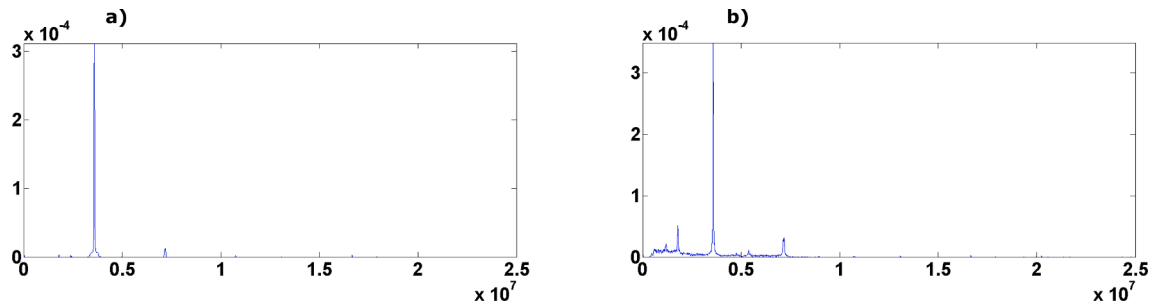

Fig. 5. Acoustic spectra at fixed frequency 3.6 MHz for different HIFU excitation voltages; 100 mV (a) and 200 mV (b).

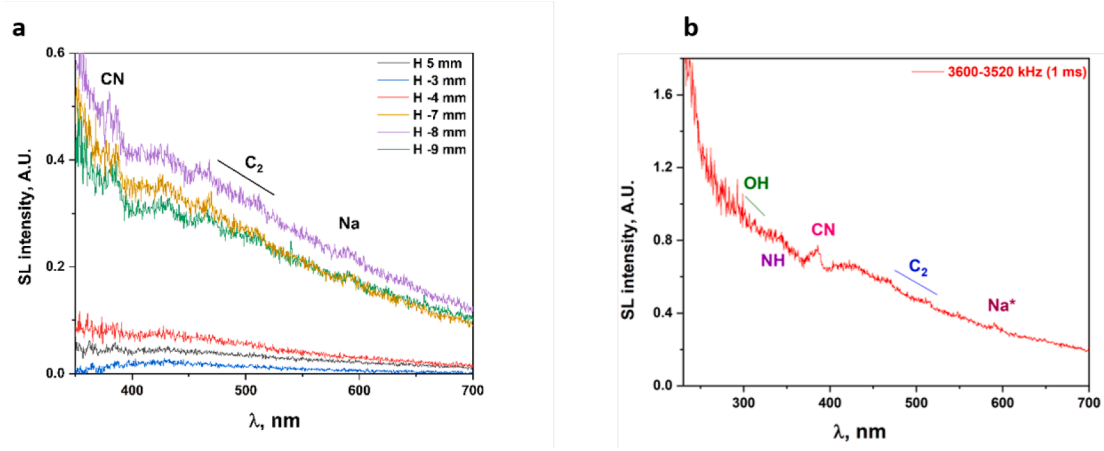

Fig. 8. (a) SL emission spectra of HIFU in wobbling mode, in 1 M NaCl + 3.7 mM 2-propanol under Ar-15.5%O_2-2.2%N_2 at 3600–3520 kHz (1 ms) at different heights H. (b) SL emission spectra of HIFU in wobbling mode, in 1 M NaCl + 3.7 mM 2-propanol under Ar-15.5%O_2-2.2%N_2 at f = 3600–3520 kHz, −80 MHz/s (1 ms), merged with the corresponding spectra using high-pass filter 320 nm.

emission was in keeping with its reported decrease with frequency [45]. As for broadening of molecular emissions, it was observed to increase with US frequency [14,46] and was attributed to Stark effect, i.e. broadening of emissions by the charged particles in the plasma [46].

Fig. 7 presents SL emission spectra measured using these optimized conditions of solution and gas in the pre- and post- focal zones, so at different heights based on Fig. 2a. Results indicate that the SL of the pre-focal zone is brighter and more intense than in the zone above, in accordance with the observations with SCL (Figs. 2a and 8a). Besides, Fig. 8a and Fig. 4SI in Supporting information show that the spectra of both zones are similar in shape, with the same continuum and molecular emissions, which would indicate that a similar plasma is formed in the different bubbles. Molecular emissions must be simulated to confirm this observation. Since SL emission spectra on both pre- and post- focal zones overlap once normalized (Fig. 4SI in Supporting information), the study of the impact of wobbling parameters was mostly conducted in the zone of higher intensity.

3.3. SL emission spectroscopy in sweep mode

First parameter of interest is F_{start}. A series of experiments was carried out for different F_{start} between 3.28 and 4.0 MHz using positive and negative sweeps ($\Delta F > 0$ and $\Delta F < 0$), a constant absolute sweep rate of 80 MHz /s, and a sweep time of 1 ms. As seen in Fig. 9, the SL emission spectra were most intense for F_{start} between 3.6 MHz and 3.88 MHz. Interestingly, changing initial frequency does not seem to impact the shape of the SL spectra: all spectra are similar and overlap if normalized, despite very different intensities: no large spectral difference is observed either in the continuum shape or in CN emission.

Sweep time is another important factor in wobbling, as shown in previous works where global SCL/SL intensities were extensively studied [29,30]. For this reason, a number of experiments were carried out with a starting frequency of 3.6 MHz, a sweep rate of ±80 MHz/s, and different sweep times from 1 ms to 5 ms with a 1 ms step size. Sweep frequency interval width thus varied from ±80 to ±400 kHz. Fig. 10 presents spectra measured in the pre-focal zone with different wobbling times, a constant rate of −80 MHz/s, and a starting frequency of 3.6 MHz. The highest intensity is obtained for 3600–3440 kHz ($\Delta F = -160$ kHz). No spectral difference is observed when changing sweep time. Spectra measured in the post-focal zone are presented in Fig. 5SI in Supporting information. The most intense ones are obtained for a sweep time of 1 ms (3.6–3.52 MHz) with an intensity much larger than for

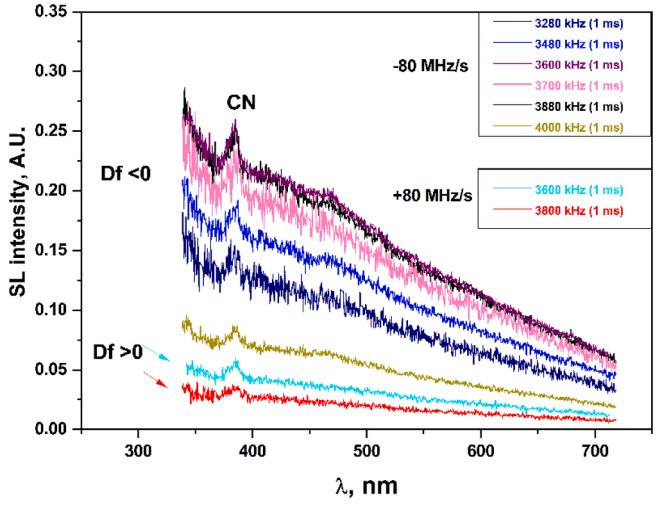

Fig. 9. SL emission spectra of HIFU in wobbling mode, in 1 M NaCl + 3.7 mM 2-propanol under Ar-15.5%O_2-2.2%N_2 at a sweep rate of ±80 MHz/s and a sweep time of 1 ms, for different F_{start} at H 7 mm.

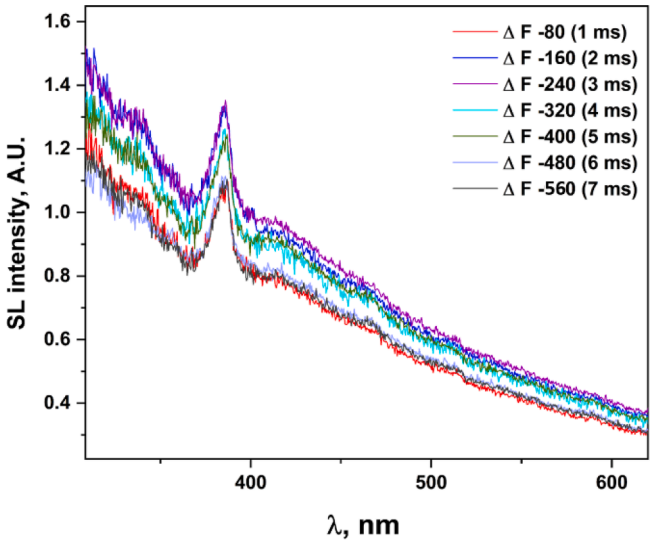

Fig. 10. SL emission spectra of HIFU in wobbling mode, in 1 M NaCl + 3.7 mM 2-propanol under Ar-15.5%O_2-2.2%N_2 at F_{start} = 3600 kHz, −80 MHz/s at different sweep times, H −8 mm, merged with the corresponding spectra using a high-pass filter.

other wobbling periods. This observation tallies with the trend followed by SCL (Fig. 2b), for both pre- and post-focal zones.

Finally, the influence of sweep rate on SL spectra was studied: Fig. 11a shows SL emission spectra at 3.6–3.44 MHz with a sweep time ranging from 1 to 3.5 ms with a step of 0.5 ms, corresponding to the sweep rates 160, 106.7, 80, 64, 53.3 and 45.7 MHz/s, respectively. The most intense spectra are obtained at the rate of −80 MHz/s. Besides, spectra are similar in shape and superimpose if a scaling factor is used, as illustrated in Fig. 11b for the rates −80, −53.3 and −160 MHz/s.

These comparisons of spectra measured in different wobbling conditions indicate that the formed intra-bubble plasma is similar. In this case, the very different light intensities are to be attributed to a different number of emitting bubbles or, in other words, to different bubble densities.

3.4. Simulations

Most observed molecular emissions at the very high frequencies of 3.6–4 MHz are too weak and broad to be properly fitted: the signal-to-noise ratio is too low. Only CN emission is intense enough to be fitted. Fig. 12 presents this emission after removal of a baseline corresponding to SL continuum and normalization, for a sweep between 3600 and 3360 kHz in 3 ms, and its simulation using Specair software. The obtained vibrational temperature T_v is 10000 ± 2000 K, the rotational temperature T_r 7000 ± 2000 K, and the effective pressure 14000 ± 2000 bar. As previously discussed [46], this value reflects the broadening due to pressure and Stark effects. It was checked that all experimental spectra (with different sweep times and different sweep rates) can be fitted with these values, confirming that the variation in SL intensity in the different wobbling conditions is due to a variation in the number of active bubbles, while the formed intra-bubble plasma does not seem to be impacted. For comparison, Fig. 12 also presents CN emission obtained at 1057 kHz in 1 M NaCl 3.7 mM 2-propanol saturated with Ar-15.5%O_2-2.2%N_2 and its Specair simulation (the whole SL spectrum at 1057 kHz is given in Fig. 6SI in Supporting Information). Obtained rovibronic temperatures are T_v = 8000 ± 2000 K, T_r = 6000 ± 2000 K, and effective pressure 12000 ± 2000 bar. The latter values are very similar to those obtained using HIFU at 3.6 MHz under sweeping conditions. This comparison confirms the general trend previously reported for frequencies in the range 20–1000 kHz [46], namely a very large increase in the broadening of molecular emissions, traced back to an increase in ionization degree of the plasma. In this case, the trend is extrapolated to very high frequencies and to focused geometry and sweeping.

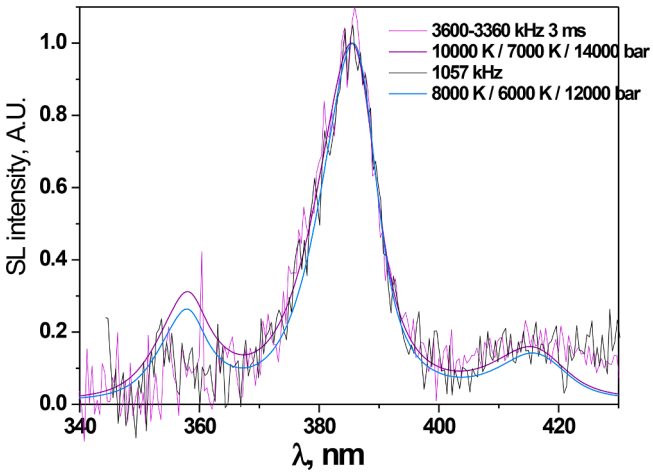

Fig. 12. CN emission in 1 M NaCl 3.7 mM 2-propanol saturated with Ar-15.5% O_2-2.2%N_2, for a frequency sweep between 3600 and 3360 kHz (3 ms) and at 1057 kHz, and corresponding simulations using Specair software.

4. Conclusion

This study proved once again that sweeping HIFU frequency is a powerful tool for controlling cavitation activity. SCL results allow mapping of intensity and distribution of the HIFU acoustic field, where the pre-focal zone is confirmed as the brighter one. However, activation of the post-focal zone is possible by applying very short sweeping periods of 1 ms. Integration of the area below acoustic spectra curves at different wobbling parameters (rsweep, Tsweep and ΔF) confirms SCL measurements by showing the same attenuation (positive scan) or intensification (negative scan) of cavitational activity. In 1 M NaCl 3.7 mM 2-propanol solution saturated by a mixture of Ar-15.5%O_2-2.2%N_2, intensities of SL spectrum are high enough to allow detection of several molecular emissions under negative frequency sweeps of 3.6–3.52 MHz, −80 MHz/s (1 ms). Molecular emissions of OH, NH, C_2, Na are detected. Their intensities are low, and they are very broad, following the same trend obtained at fixed frequencies up to 1 MHz. Under optimized conditions, CN emission is strong enough to be simulated, which is reported for the first time at such high frequency. Its resulting vibrational temperature T_v of 10000 ± 2000 K, rotational temperature of T_r 7000 ± 2000 K, and effective pressure of 14000 ± 2000 bar are of the same range of magnitude as those at 1 MHz. In particular, the effective pressure value indicates that plasma is ionized to the same extent as in

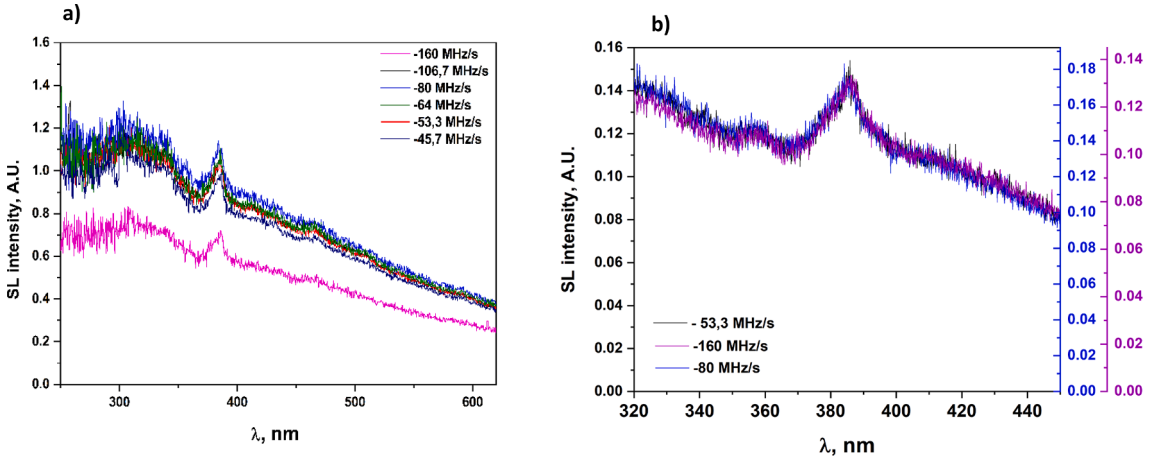

Fig. 11. SL emission spectra of HIFU in wobbling mode, in 1 M NaCl + 3.7 mM 2-propanol under Ar-15.5%O_2-2.2%N_2 at F_{start} = 3600 kHz, at different sweep times and rates, H −8 mm. The grating 150blz500 is used in graph a, while graph b shows the results with the 600blz300 grating chosen to stress the identical shape of CN emission and continuum.

the usual high frequency range. The fact that no spectral difference is detected indicates that bubble nature is the same in the pre- and post-focal zones under different sweeping parameters, and that the only difference is intensity. Consequently, SL and SCL intensification is not related to a change in plasma nature inside the bubbles but to the number of cavitation bubbles.

Declaration of Competing Interest

The authors declare that they have no known competing financial interests or personal relationships that could have appeared to influence the work reported in this paper.

Acknowledgements

The authors gratefully acknowledge the IRT M2P Metz for its financial support (projects RESEM VOBUSURF and SPECTRUSEB).

Appendix A. Supplementary data

Supplementary data to this article can be found online at https://doi.org/10.1016/j.ultsonch.2022.105939.

References

[1] K.S. Suslick, Sonochemistry, Science (80-) 247 (4949) (1990) 1439–1445.
[2] E.B. Flint, K.S. Suslick, The temperature of cavitation, Science (80-) 253 (5026) (1991) 1397–1399.
[3] Y.T. Didenko, W.B. McNamara, K.S. Suslick, Hot spot conditions during cavitation in water, J. Am. Chem. Soc. 121 (24) (1999) 5817–5818.
[4] M. Ashokkumar, F. Grieser, A comparison between multibubble sonoluminescence intensity and the temperature within cavitation bubbles, J. Am. Chem. Soc. 127 (15) (2005) 5326–5327.
[5] H. Xu, N. Glumac, K. Suslick, Temperature inhomogeneity during multibubble sonoluminescence, Angew. Chem. Int. Ed. 49 (6) (2010) 1079–1082.
[6] R. Ji, R. Pflieger, M. Virot, S.I. Nikitenko, Multibubble Sonochemistry and Sonoluminescence at 100 kHz: The Missing Link between Low- and High-Frequency Ultrasound, J. Phys. Chem. B 122 (2018) 6989–6994.
[7] F. Lepoint-Mullie, N. Voglet, T. Lepoint, R. Avni, Evidence for the emission of "alkali-metal-noble-gas" van der Waals molecules from cavitation bubbles, Ultrason. Sonochem. 8 (2) (2001) 151–158.
[8] K.S. Suslick, E.B. Flint, Sonoluminescence from non-aqueous liquids, Nature 330 (6148) (1987) 553–555.
[9] J. Rooze, E.V. Rebrov, J.C. Schouten, J.T.F. Keurentjes, Dissolved gas and ultrasonic cavitation – A review, Ultrason. Sonochem. 20 (1) (2013) 1–11.
[10] R. Pflieger, T. Chave, G. Vite, L. Jouve, S.I. Nikitenko, Effect of operational conditions on sonoluminescence and kinetics of H_2O_2 formation during the sonolysis of water in the presence of Ar/O_2 gas mixture, Ultrason. Sonochem. 26 (2015) 169–175.
[11] R. Pflieger, L. Gravier, G. Guillot, M. Ashokkumar, S.I. Nikitenko, Inverse effects of the gas feed positioning on sonochemistry and sonoluminescence, Ultrason. Sonochem. 46 (2018) 10–17.
[12] R. Pflieger, S.I. Nikitenko, M. Ashokkumar, Effect of NaCl salt on sonochemistry and sonoluminescence in aqueous solutions, Ultrason. Sonochem. 59 (2019) 104753, https://doi.org/10.1016/j.ultsonch.2019.104753.
[13] K.S. Suslick, Sonoluminescence and sonochemistry, Proc. IEEE Ultrason. Symp. 1 (1997) 523–532.
[14] R. Pflieger, A.A. Ndiaye, T. Chave, S.I. Nikitenko, Influence of ultrasonic frequency on Swan band sonoluminescence and sonochemical activity in aqueous tert-butyl alcohol solutions, J. Phys. Chem. B. 119 (1) (2015) 284–290.
[15] S. Hirayama, H. Morinaga, T. Ohmi, J.-I. Soejima, Sonoluminescence measurement of 1 MHz ultrasonic cavitation and effect of dissolved gases, Acoust. Sci. Technol. 29 (6) (2008) 345–350.
[16] K. Yasui, K. Kato, Bubble dynamics and sonoluminescence from helium or xenon in mercury and water, Phys. Rev. E 86 (2012) 1–11.
[17] S.I. Nikitenko, R. Pflieger, Toward a new paradigm for sonochemistry: Short review on nonequilibrium plasma observations by means of MBSL spectroscopy in aqueous solutions, Ultrason. Sonochem. 35 (2017) 623–630.
[18] F.R. Young, Sonoluminescence, first ed., CRC Press, 2004.
[19] R. Pflieger, E. Fayard, C. Noel, S.I. Nikitenko, T. Belmonte, Molecular emissions in sonoluminescence spectra of water sonicated under Ar-based gas mixtures, Ultrason. Sonochem. 58 (2019) 104637, https://doi.org/10.1016/j.ultsonch.2019.104637.
[20] M.A. Beckett, I. Hua, Impact of Ultrasonic Frequency on Aqueous Sonoluminescence and Sonochemistry, J. Phys. Chem. A 105 (15) (2001) 3796–3802.
[21] K. Yasui, Influence of ultrasonic frequency on multibubble sonoluminescence, J. Acoust. Soc. Am. 112 (4) (2002) 1405–1413.
[22] P. Kanthale, M. Ashokkumar, F. Grieser, Sonoluminescence, sonochemistry (H_2O_2 yield) and bubble dynamics: Frequency and power effects, Ultrason. Sonochem. 15 (2) (2008) 143–150.
[23] R.A. Fowler, S.L. Fossheim, J.-L. Mestas, J. Ngo, E. Canet-Soulas, C. Lafon, Non-invasive Magnetic Resonance Imaging Follow-up of Sono-sensitive Liposome Tumor Delivery and Controlled Release After High-Intensity Focused Ultrasound, Ultrasound Med. Biol. 39 (12) (2013) 2342–2350.
[24] P. Gélat, G. ter Haar, N. Saffari, The optimization of acoustic fields for ablative therapies of tumours in the upper abdomen, Phys. Med. Biol. 57 (24) (2012) 8471–8497.
[25] L. Hallez, F. Touyeras, J.Y. Hihn, Y. Bailly, H.I.F.U. Interactions, / polymer films, Phys. Proc. 3 (2010) 179–184.
[26] L. Hallez, F. Touyeras, J.Y. Hihn, J. Klima, J.L. Guey, M. Spajer, Y. Bailly, Characterization of HIFU transducers designed for sonochemistry application: Cavitation distribution and quantification, Ultrasonics 50 (2010) 310–317.
[27] L. Hallez, F. Touyeras, J.-Y. Hihn, Y. Bailly, Characterization of HIFU transducers designed for sonochemistry application: Acoustic streaming, Ultrason. Sonochem. 29 (2016) 420–427.
[28] H. Chen, X. Li, M. Wan, S. Wang, High-speed observation of cavitation bubble cloud structures in the focal region of a 1.2 MHz high-intensity focused ultrasound transducer, Ultrason. Sonochem. 14 (3) (2007) 291–297.
[29] J. Lee, M. Ashokkumar, S. Kentish, F. Grieser, Determination of the size distribution of sonoluminescence bubbles in a pulsed acoustic field, J. Am. Chem. Soc. 127 (48) (2005) 16810–16811.
[30] J. Lee, L. Hallez, F. Touyeras, M. Ashokkumar, J.-Y. Hihn, Influence of frequency sweep on sonochemiluminescence and sonoluminescence, Ultrason. Sonochem. 64 (2020) 105047, https://doi.org/10.1016/j.ultsonch.2020.105047.
[31] L. Hallez, J. Lee, F. Touyeras, A. Nevers, M. Ashokkumar, J.-Y. Hihn, Enhancement and quenching of high-intensity focused ultrasound cavitation activity via short frequency sweep gaps, Ultrason. Sonochem. 29 (2016) 194–197.
[32] L. Hallez, F. Touyeras, J.Y. Hihn, J. Klima, Energetic balance in an ultrasonic reactor using focused or flat high frequency transducers, Ultrason. Sonochem. 14 (6) (2007) 739–749.
[33] H. Chen, X. Li, M. Wan, The inception of cavitation bubble clouds induced by high-intensity focused ultrasound, Ultrasonics 44 (2006) e427–e429.
[34] H. Chen, X. Li, M. Wan, Spatial-temporal dynamics of cavitation bubble clouds in 1.2 MHz focused ultrasound field, Ultrason. Sonochem. 13 (6) (2006) 480–486.
[35] S.I. Nikitenko, M. Brau, R. Pflieger, Acoustic noise spectra under hydrothermal conditions, Ultrason. Sonochem. 67 (2020) 105189, https://doi.org/10.1016/j.ultsonch.2020.105189.
[36] I. Tzanakis, G.S.B. Lebon, D.G. Eskin, K.A. Pericleous, Characterizing the cavitation development and acoustic spectrum in various liquids, Ultrason. Sonochem. 34 (2017) 651–662.
[37] N.V. Dezhkunov, A. Francescutto, L. Serpe, R. Canaparo, G. Cravotto, Sonoluminescence and acoustic emission spectra at different stages of cavitation zone development, Ultrason. Sonochem. 40 (2018) 104–109.
[38] C. Desjouy, P. Labelle, B. Gilles, J.-C. Bera, C. Inserra, Orbital trajectory of an acoustic bubble in a cylindrical resonator, Phys. Rev. E 88 (3) (2013), https://doi.org/10.1103/PhysRevE.88.033006.
[39] A. Sabraoui, C. Inserra, B. Gilles, J.-C. Béra, J.-L. Mestas, Feedback loop process to control acoustic cavitation, Ultrason. Sonochem. 18 (2) (2011) 589–594.
[40] F.R. Young, Sonoluminescence from water containing dissolved gases, J. Acoust. Soc. Am. 60 (1) (1976) 100–104.
[41] R. Pflieger, J. Lee, S.I. Nikitenko, M. Ashokkumar, Influence of He and Ar Flow Rates and NaCl Concentration on the Size Distribution of Bubbles Generated by Power Ultrasound, J. Phys. Chem. B 119 (39) (2015) 12682–12688.
[42] S. Kumari, M. Keswani, S. Singh, M. Beck, E. Liebscher, P. Deymier, S. Raghavan, Control of sonoluminescence signal in deionized water using carbon dioxide, Microelectron. Eng. 88 (12) (2011) 3437–3441.
[43] C. Wang, N. Srivastava, OH number densities and plasma jet behavior in atmospheric microwave plasma jets operating with different plasma gases (Ar, Ar/N2, and Ar/O 2), Eur. Phys. J. D 60 (3) (2010) 465–477.
[44] R.J. Wood, J. Lee, M.J. Bussemaker, A parametric review of sonochemistry: Control and augmentation of sonochemical activity in aqueous solutions, Ultrason. Sonochem. 38 (2017) 351–370.
[45] C. Cairós, J. Schneider, R. Pflieger, R. Mettin, Effects of argon sparging rate, ultrasonic power, and frequency on multibubble sonoluminescence spectra and bubble dynamics in NaCl aqueous solutions, Ultrason. Sonochem. 21 (6) (2014) 2044–2051.
[46] R. Pflieger, T. Ouerhani, T. Belmonte, S.I. Nikitenko, Use of NH (A3Π-X3Σ-) sonoluminescence for diagnostics of nonequilibrium plasma produced by multibubble cavitation, Phys. Chem. Chem. Phys. 19 (38) (2017) 26272–26279.